Materials and Design 139 (2018) 314–323

Contents lists available at ScienceDirect

Materials and Design

journal homepage: www.elsevier.com/locate/matdes

Role of Mn and Cr on structural parameters and strain energy during FCC-HCP martensitic transformation in Fe-Mn-Cr shape memory alloys

F. Malamud [a,b], L.M. Guerrero [a,b], P. La Roca [a,b], M. Sade [a,b,*], A. Baruj [a,b]

[a] Centro Atómico Bariloche (CNEA) and Instituto Balseiro (U.N. Cuyo – CNEA), Av. Bustillo 9500, 8400 Bariloche, Argentina
[b] CONICET, Argentina

HIGHLIGHTS

- Structural parameters of FCC, HCP and BCC phases of Fe-Mn-Cr alloys were measured in an extended chemical composition range.
- Mn additions tend to increase lattice parameters in these alloys.
- Volume changes of FCC/HCP transformation decrease as Cr content increases.
- The strain energy barrier to the FCC-HCP martensitic transformation decreases as Cr content increases.

GRAPHICAL ABSTRACT

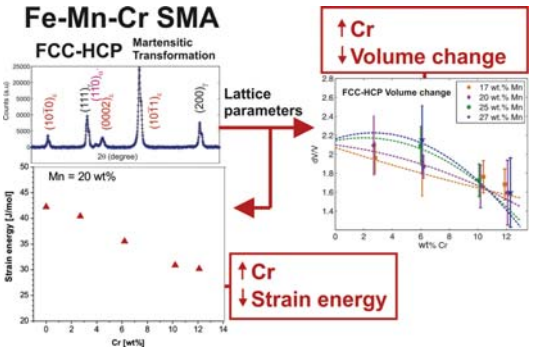

ARTICLE INFO

Article history:
Received 30 August 2017
Received in revised form 7 November 2017
Accepted 9 November 2017
Available online 10 November 2017

Keywords:
Fe-Mn-Cr
Martensitic transformations
Volume change
Lattice parameters
Strain energy

ABSTRACT

Fe-Mn-based alloys show the shape memory effect which is mainly related to the FCC-HCP martensitic transformation. Cr is one of the additional elements which improve the properties of these alloys. In the present work structural data are obtained for the FCC austenite, and both martensitic structures, HCP and BCC, for an extended composition range where the FCC-HCP transition takes place. Lattice parameters are determined by X-Ray diffraction measurements performed at room temperature. The volume change between the austenite and each martensitic structure plays a significant role on relevant properties for martensitic transformations, like the strain energy associated to the transition. The effect of Mn and Cr on lattice parameters and volume change between FCC and HCP is determined and modeling of the data is presented. This result allows estimating the strain energy associated to the phase change. By using this information, the strain energy contribution to the balance of energy for the HCP nucleation is discussed. The addition of Cr decreases the volume change between FCC and HCP for contents larger than 12 wt% Cr which leads to a decrease of the strain energy. Both effects favor an increased shape memory effect associated to the FCC-HCP martensitic transition.

1. Introduction

Fe-Mn-based alloys are attractive due to the shape memory effect (SME). In these alloys the SME is related to the FCC-HCP martensitic transformation. The SME has been optimized in Fe-Mn-Si-Cr-Ni alloys where a fully reversible 8% deformation has been obtained [1]. This property in addition to the low nominal cost of these steels makes them promising candidates for technological applications [2,3]. Large recovery strains have been reported in Fe-Mn-based alloys containing multiple elements. However, there is a lack of knowledge on the effect of each element on structural and functional properties.

* Corresponding author.
E-mail address: sade@cab.cnea.gov.ar (M. Sade).

https://doi.org/10.1016/j.matdes.2017.11.017
0264-1275/

Cr, in particular, is an element usually added to obtain oxidation and corrosion resistance [4–6]. Previous reports indicate that Cr could also affect the stacking fault energy of Fe-Mn-based alloys in a different way than other additions like Si or Co [6]. This is important because the SME of Fe-Mn-Cr alloys is associated to the stacking fault energy of this system [7,8].

Considering the Fe-Mn rich corner of the Fe-Mn-Cr phase diagram [9,10] and depending on the chemical composition, three phases are mainly present in quenched alloys: an austenitic phase with a FCC structure (γ), a martensitic phase with a HCP structure (ε) and a martensitic phase with a BCC structure (α') [11–15]. Quenched alloys containing over 13 wt% of Cr might contain the Fe-Cr σ phase [9,16]. The martensitic transformation temperatures in this alloy system depend on the chemical composition and on the thermomechanical history of the material [7,15,17].

The relevance of the FCC-HCP martensitic transformation on the properties of Fe-Mn-Cr alloys is not limited to the shape memory effect. Fe-Mn-Cr-based alloys display transformation induced plasticity (TRIP) [13] and twinning induced plasticity (TWIP) [18–20] which provide them outstanding formability. Fe-Mn-Cr alloys were also proposed as cryogenic steels [21–23] and as structural Ni-free stainless steels [11, 12,21,24–26]. In the case of cryogenic applications it is convenient to inhibit the martensitic transformation thus retaining the austenite down to very low temperatures. This requires the comprehension of the role played by each element on the relative phase stability among the structures potentially present.

One of the main obstacles to precisely determine the effect of each component of the alloys on materials properties is that most of previously published studies involve either commercial grade steels or Fe-Mn-Cr steels containing C, N, Si and/or additional elements [11–13, 20–24,26–33]. In comparison, not much work has been reported on the pure Fe-Mn-Cr ternary system. In a previous work, present authors reported the effect of Cr on the FCC-HCP martensitic transformation temperatures and on the Néel transition temperature of the FCC structure [15]. The analysis of the FCC-HCP transformation requires a precise knowledge of the magnetic ordering temperatures since the para-antiferromagnetic transition of the FCC structure strongly stabilizes this phase altering the Gibbs free energy change between FCC and HCP structures [34].

One of the most relevant properties concerning martensitic phase transformations is the volume change between the involved phases. Diffusion-less phase transformations involving large volume changes, as it is the case here, require the introduction of plastic deformation in the material in order to accommodate the associated distortion. This plastic deformation directly affects the reversibility of the involved shape changes, promoting or inhibiting the SME. It also plays a prominent role in materials designed to obtain the TRIP or TWIP effects. In fact, if the volume change were strongly reduced, the possibility of attaining a degree of thermoelasticity and pseudoelasticity could be increased, as it is known to occur in Cu- and NiTi-based alloys [35–38]. Very small volume changes are key to get pseudoelastic properties in Fe-Mn-Al-Ni alloys, as it has been recently reported [39,40], this finding has been extremely noticeable and relevant [41–46]. One of the purposes of the present work is to evaluate the effect of composition on the volume change in the Fe-Mn-Cr system in the composition range where the FCC-HCP and reverse transitions take place. To accomplish this aim, precise measurements of the lattice parameters of the involved structures are required.

Structural information about BCC, FCC and HCP phases in the Fe-Mn-Cr system is scarce. There is some information about the lattice parameters of these phases but, in most cases, the studies have been performed on low purity alloys or on alloys where appreciable quantities of additional elements have been added on purpose [32]. As far as we know, the only experimental information on the lattice parameters of the FCC phase of Fe-Mn-Cr alloys is included in a work by Reeh et al. where thin films with different compositions were prepared by combinatorial sputtering method [47], and in an extended study from Rawers [32]. Data from Reeh comprise an array of alloys with about 29% Mn and 4% to 6% Cr where the austenite lattice parameter is almost constant ($a_{FCC} \approx 0.36$ nm). Rawers' data include 5 alloys containing from 14.6 wt% Mn to 24.5 wt% Mn and from 14.3 wt% Cr to 16.4 wt% Cr, obtaining similar FCC lattice parameters, although a tendency to increase the lattice parameter with the increment of Mn amount is observed. In addition, Tamarat et al. informed the lattice parameter of the BCC phase for a single alloy containing 14.1% Mn and 12.4% Cr ($a_{BCC} = 0.286$ nm) [48].

As it was stated before, the volume change directly affects the strain energy involved in the FCC-HCP transformation. It is necessary to have information about this magnitude for the analysis of the nucleation of the HCP phase. According to the widely used model from Olson and Cohen, a stacking fault formed by the dissociation of a perfect dislocation in FCC, which has a stacking sequence corresponding to the basal plane of the HCP structure, becomes an HCP embryo [49]. When the driving force for the transformation is large enough to compensate the required strain energy and the surface energy, the embryo becomes an HCP nucleus and it can grow, enabling the transformation. This model has been widely applied to analyze this kind of transformation in a variety of systems. It is remarkable that the mentioned energetic barriers, i.e. the strain energy and the surface energy are enough to understand the mechanism of nucleation and growth of the HCP structure in a FCC matrix [49,50]. Considering Fe-Mn-Cr alloys, there is no systematic and sufficient available data on the lattice parameters which could be used to estimate the effect of Cr on the volume change associated to the martensitic transformations and the strain energy.

In view of these problems, we have performed systematic X-Ray diffraction (XRD) experiments in order to measure the lattice parameters of Fe-Mn-Cr alloys in a wide composition range where the FCC/HCP transformation takes place. With these data, volume changes are obtained, the strain energy is calculated and its magnitude compared with Gibbs free energy changes reported in the literature.

2. Experimental procedure

Seventeen Fe-Mn-Cr alloys have been prepared for the present work. The alloys were arc melted starting with pure metals (purity 99.98 Fe, 99.9 Mn and 99.9 Cr). Each alloy was melted and turned upside down several times under Ar atmosphere and buttons of approximately 15 g were obtained. The resulting alloys were homogenized by a heat-treatment in quartz capsules under Ar atmosphere for 48 h at 1273 K and water quenched by breaking the capsules. The chemical composition of each alloy was determined by the neutron activation technique in the RA-6 experimental nuclear reactor at Centro Atómico Bariloche [34]. The resulting compositions are summarized in Table 1.

Considering the Fe-Mn system as a starting point, Mn contents of these alloys include most of the compositions where the HCP structure can be thermally induced. The alloy with the lowest Mn content (Alloy 1 containing 13.7 wt% Mn) corresponds to a composition where only the BCC martensite is found in the Fe-Mn system. On the other end of the Table, alloys with the highest Mn contents (Alloys 16 and 17) correspond to those cases where the magnetic ordering of the FCC structure occurs at temperatures higher than that of the martensitic transformation in the Fe-Mn system. The selected Cr composition range, from 2.1 wt% up to 12.4 wt% allows the formation of thermally induced HCP martensite as it was previously reported [15].

Metallographic observations were performed on the samples. Austenite grain sizes were determined by applying the intercept line method to the micrographs, following the procedure described in the ASTM E112-12 standard.

XRD specimens were cut from the quenched buttons using a spark erosion machine. The samples of approximately 1 mm × 4 mm × 12 mm were polished using 600 and 1200 grit emery papers, individually encapsulated into quartz tubes under Ar atmosphere, annealed for

Table 1
Alloy denomination, measured chemical composition, measured lattice parameters and goodness of fit factor for all studied Fe-Mn-Cr alloys. The BCC phase could not be detected by XRD means in those samples where a lattice parameter for this phase is not informed.

Alloy	wt% Mn (±0.4%)	wt% Cr (±0.1%)	a_{FCC}(Å)	a_{HCP}(Å)	c_{HCP}(Å)	a_{BCC}(Å)	R (%)
1	13.7	2.6	3.588 ± 0.002	2.5325 ± 0.0003	4.0820 ± 0.0007	2.8759 ± 0.0008	3.50
2	16.7	10.4	3.5973 ± 0.0009	2.538 ± 0.001	4.099 ± 0.001	2.877 ± 0.002	4.37
3	17.1	11.9	3.601 ± 0.001	2.5415 ± 0.0001	4.105 ± 0.002		8.91
4	17.3	6.1	3.595 ± 0.002	2.535 ± 0.001	4.094 ± 0.003	2.875 ± 0.0007	4.80
5	17.9	2.8	3.592 ± 0.001	2.5339 ± 0.0007	4.087 ± 0.002		5.88
6	19.1	10.1	3.598 ± 0.002	2.5395 ± 0.0008	4.104 ± 0.002	2.877 ± 0.002	5.57
7	19.6	12.1	3.603 ± 0.003	2.5436 ± 0.0006	4.108 ± 0.001	2.880 ± 0.003	5.13
8	19.8	10.2	3.599 ± 0.002	2.5400 ± 0.0008	4.1034 ± 0.0006		4.81
9	20	6.2	3.5965 ± 0.0006	2.5365 ± 0.0006	4.098 ± 0.001		5.64
10	20.7	2.7	3.596 ± 0.002	2.536 ± 0.002	4.091 ± 0.002		6.38
11	21	12.4	3.605 ± 0.002	2.5440 ± 0.0005	4.109 ± 0.001		6.08
12	22.9	10.7	3.602 ± 0.003	2.542 ± 0.002	4.106 ± 0.003		5.69
13	24.3	10.1	3.605 ± 0.001	2.5433 ± 0.0007	4.1102 ± 0.0005		7.55
14	24.7	2.1	3.601 ± 0.002	2.537 ± 0.002	4.093 ± 0.003		6.67
15	24.9	6	3.602 ± 0.002	2.5388 ± 0.0005	4.101 ± 0.001		5.47
16	27.1	12.3	3.610 ± 0.003	2.5480 ± 0.0009	4.118 ± 0.002		4.81
17	27.5	6.1	3.605 ± 0.001	2.540 ± 0.002	4.105 ± 0.005		6.65

1 h at 1273 K and water quenched by breaking the capsules. Before the measurements all samples were chemically polished with a solution of 90 vol% H_2O_2 – 5 vol% HF – 5 vol% HNO_3 for about 40 s in order to remove any surface deformations produced by the sample preparation method.

XRD measurements have been performed at 295 K (room temperature), using a Bruker D8 Advance X-ray diffractometer with a synchronous rotation holder. The diffractometer is equipped with a Cu anode, a fast counting detector based on Silicon strip technology (Bruker Lynx Eye line detector) and a Ni filter. It was operated with a current of 40 mA and a voltage of 40 kV and the selected slit size was 1 mm to take full advantage of the line detector. The martensitic transformation temperatures of each sample were measured previously, as reported in Ref. [15]. In this way, by cooling or heating the samples, the phases FCC and HCP were obtained at room temperature in all X-Ray measurements.

3. Results and discussion

3.1. Alloys microstructure

An example of the observed microstructures is presented in Fig. 1. The HCP martensite appears as straight lines or plates (Fig. 1a and b), while the BCC phase (when present) appears in the form of needles (Fig. 1b). The alloys presented relatively large austenitic grain sizes from 100 μm up to 1 mm.

3.2. XRD results

A typical X-ray pattern obtained is shown in Fig. 2a, in this case corresponding to Alloy 2. Three phases were present in the sample (FCC, HCP and BCC). Peaks corresponding to different phases can be very close to each other or superposed (Fig. 2b and c). Peak intensities are also affected by preferential orientation and by the grain size of the samples. A full pattern refinement has been performed where all phases were fitted simultaneously.

The resulting lattice parameters for the phases of each alloy are presented in Table 1, together with the corresponding uncertainties and goodness of the refining factors (R-factors) [51]. In all cases R-factors are below 10%. This result can be taken as an indication of the good quality of the refinement method and lends support to the reliability of present experimental results. In order to analyze the results, it is convenient to separate the BCC phase from the results obtained for FCC and HCP phases.

3.2.1. BCC phase

The BCC martensitic phase has been detected in 5 of the studied compositions (Alloys 1, 2, 4, 6 and 7). The measured values for the lattice constant a_{BCC} display a slight variation with composition. This behavior and the absolute values found for a_{BCC} are consistent with previous findings in the Fe-Mn system for alloys containing between

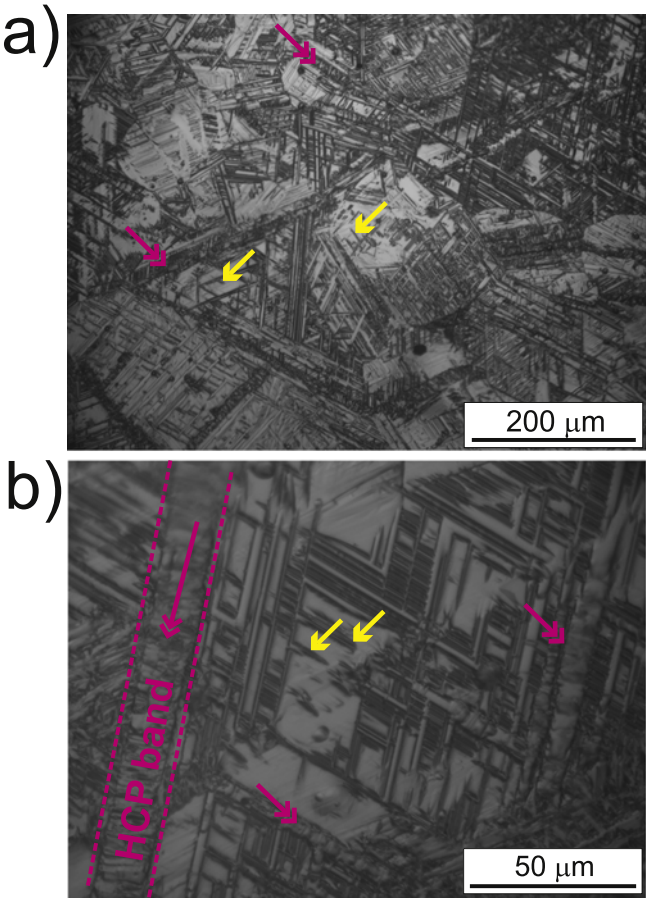

Fig. 1. a) Optical micrograph corresponding to Alloy 2. The matrix is FCC and the HCP martensite appears as straight lines (indicated with pink double arrow). b) Enlarged view of the same sample. BCC needles (indicated with yellow single arrow) can be seen in areas between HCP. (For interpretation of the references to color in this figure legend, the reader is referred to the web version of this article.)

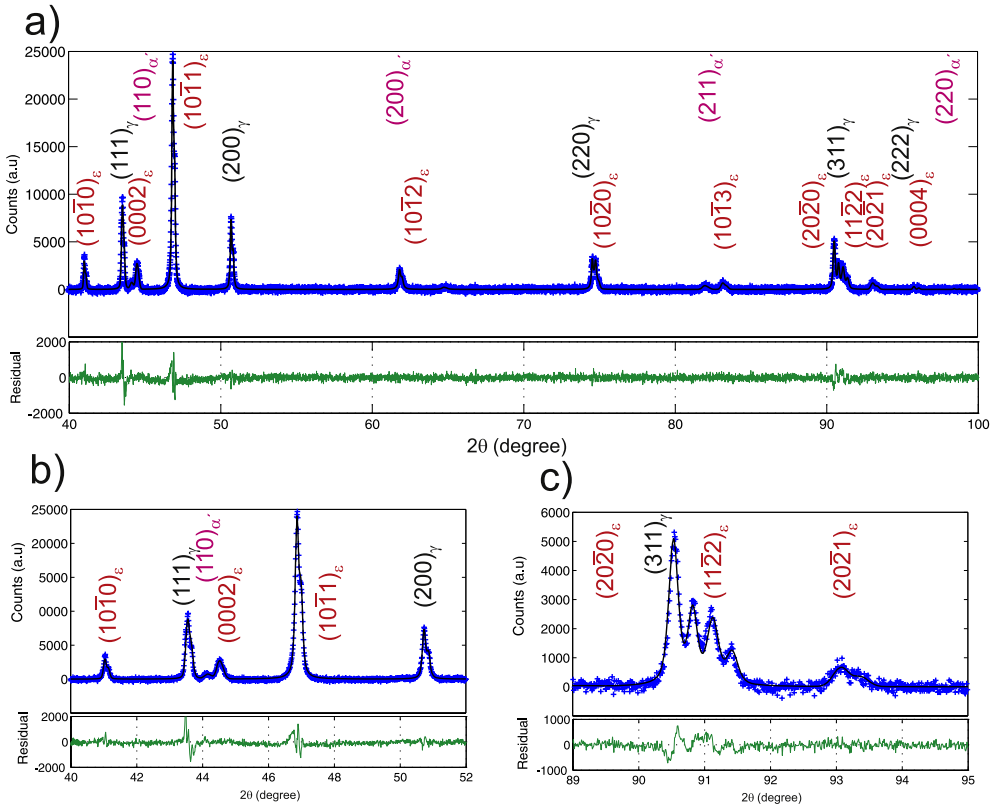

Fig. 2. a) XRD pattern measured for Alloy 2 (blue dots). Three phases are present: FCC, HCP and BCC. The black line corresponds to the data fit and the lower green line plot shows the differences between measured and fitted values. b) Detail of the 40° to 52° area of the pattern shown in a). Individual peaks corresponding to the three structures are close but can be well defined. c) Enlarged view of the area between 89° and 95° showing close or superposing peaks corresponding to different structures. A refinement method that accounts for all three phases at once is necessary to obtain meaningful data on the lattice parameters of these structures. (For interpretation of the references to color in this figure legend, the reader is referred to the web version of this article.)

13 wt% Mn and 20 wt% Mn [52]. In particular, considering the values measured for Alloys 1 and 2, it can be concluded that Cr does not cause a large effect on the lattice parameter of the BCC phase.

3.2.2. FCC and HCP phases

In order to rationalize the results presented in Table 1 for the FCC and HCP phases it is useful to group the alloys according to their approximate Cr or Mn contents. In terms of similar Cr contents, the samples can be associated in four groups: 2.5 wt% Cr (Alloys 1, 5, 10 and 14), 6 wt% Cr (Alloys 4, 9, 15 and 17), 10 wt% Cr (Alloys 2, 6, 8, 12, 13) and 12 wt% Cr (Alloys 3, 7, 11 and 16). Fig. 3 displays the results obtained for the lattice constants of the FCC (Fig. 3a) and HCP (Fig. 3b and c) phases in terms of these groups. In all cases, the lattice parameters increase with the increment of Mn content. This finding is in line with similar tendencies reported by Rawers [32] for Fe-Mn-Cr alloys. In addition, it is consistent with results reported for the Fe-Mn binary system [52,53] and ternary alloys like Fe-Mn-Co [54].

As it can be seen in Fig. 3, the variations can be approximated by linear functions (Eq. (1)). There, C_1, C_3 and C_5 are the linear coefficients and C_2, C_4 and C_6 the y-intercepts, respectively. Full lines in Fig. 3 show the results of these linear approximations for each parameter and each group of alloys.

$$\begin{cases} a_{FCC}(\text{Å}) = C_1 \times (\text{wt\%Mn}) + C_2 \\ a_{HCP}(\text{Å}) = C_3 \times (\text{wt\%Mn}) + C_4 \\ c_{HCP}(\text{Å}) = C_5 \times (\text{wt\%Mn}) + C_6 \end{cases} \quad (1)$$

As it can be observed in Fig. 3, although the lattice parameters variations can be well described by a linear function in all cases, fitted lines differ in slope and value of intercept. These differences imply that C_i values actually depend on the Cr content of the alloy. By plotting the different C_i values as a function of Cr content, we found that the dependence can be approximated by quadratic functions in all cases. Examples are shown in Fig. 4, C_1 (Fig. 4a) and C_2 (Fig. 4b), corresponding to the FCC phase, are plotted versus Cr content, being the units of C_1, C_3 and C_5, [Å/wt%] and those of C_2, C_4 and C_6, [Å].

The figure includes points corresponding to the FCC phase of the binary Fe-Mn system (i.e., 0 wt% Cr) which are shown as open symbols and were calculated from results reported in Ref. [52]. Then, a quadratic fit was performed on each C_i set of points using the expression shown in Eq. (2), where d_i are the quadratic coefficients, e_i the linear coefficients and f_i the y-intercepts, respectively.

$$C_i = d_i \times (\text{wt\%Cr})^2 + e_i \times (\text{wt\%Cr}) + f_i \quad (2)$$

The results of quadratic fits for C_1 and C_2 are displayed as full lines in Fig. 4a and b, respectively, while the values obtained for the complete set of parameters are presented in Table 2.

Now, the results presented in Table 2 can be combined with Eqs. (1) and (2) to analyze the variations of lattice parameters as a function of Cr for different contents of Mn. The results are plotted in Fig. 5a (FCC), Fig. 5b and c (HCP) as dashed lines for four different amounts of Mn.

Experimental values were included in the same graphs as solid symbols. The agreement between calculated lines and experimental values is remarkably good. Moreover, the extrapolation of the calculated lines to the Fe-Mn binary system closely match the results reported by Marinelli et al. [52,53]. This close agreement can be taken as a validation of the grouping procedure in terms of approximate Cr content and Mn content applied to the set of studied samples.

In the case of the lattice parameter of FCC, Cr additions do not show a large effect up to contents of about 5 wt%. Afterwards, further Cr

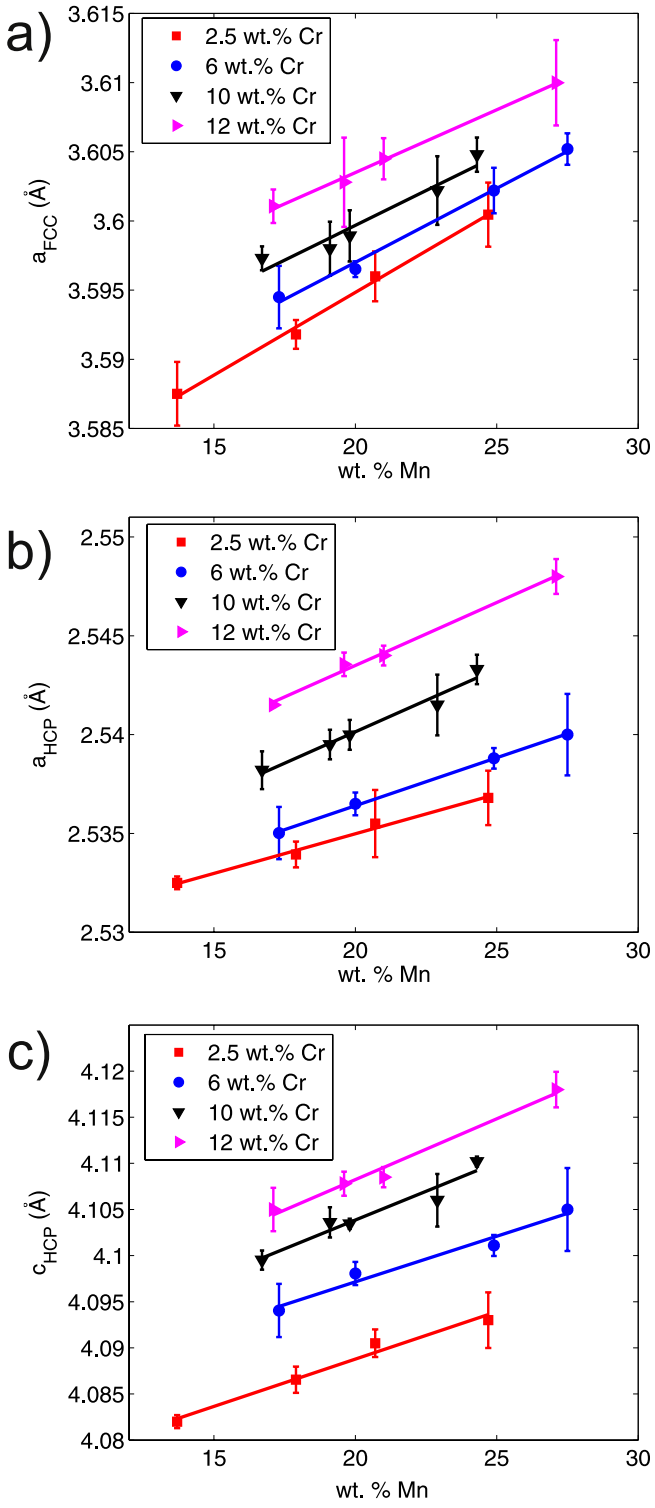

Fig. 3. Dependence of the lattice parameters as a function of the Mn content for different Cr contents. a) FCC phase lattice constant. b) and c) HCP lattice constants. The values obtained in the present work are shown in symbols, while the solid lines represent linear fits of the data following Eq. (1).

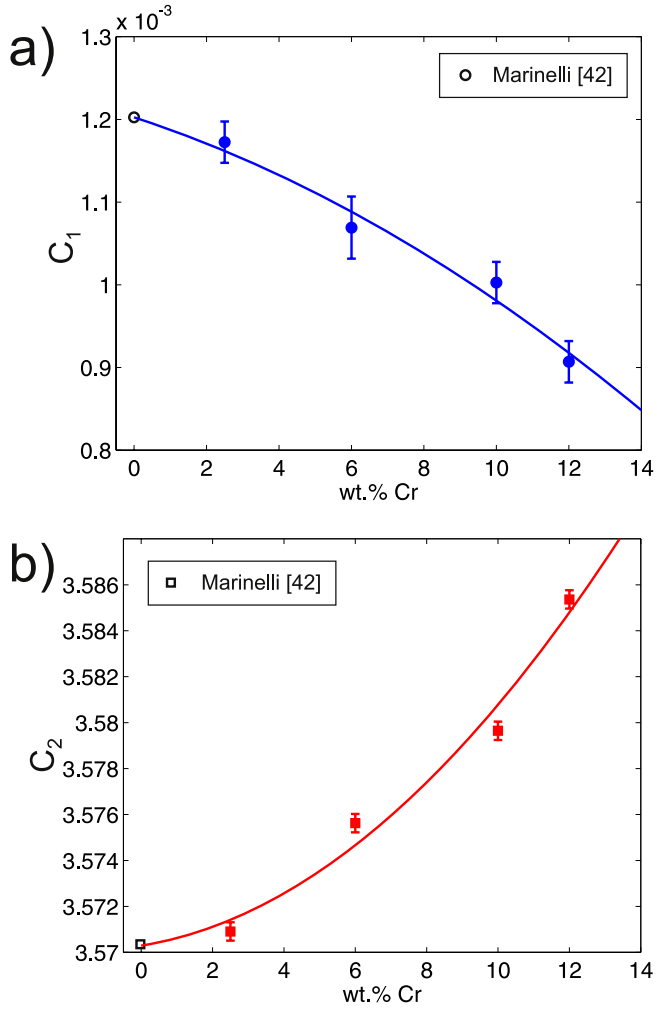

Fig. 4. Linear coefficient parameters C_1 and C_2, corresponding to the FCC phase, as a function of the Cr content. a) Parameter C_1 (circles), the open circle symbol was calculated from results reported in Ref. [52] for the binary Fe-Mn system. Full line corresponds to a quadratic fit performed using Eq. (2). b) Idem for C_2 parameters. Units of C_1 and C_2 are [Å/wt%] and [Å], respectively.

additions result in a monotonous increase of the lattice parameter. The behavior of HCP lattice parameters is more complex. While c_{HCP} parameters consistently increase with the increment of Cr amount in the alloy, the behavior of a_{HCP} parameters depend on the Mn content. Alloys with Mn concentrations of 25 wt% and 27 wt% show a minimum in a_{HCP} at about 4 wt% Cr. On the other hand, for alloys with smaller Mn contents a_{HCP} monotonously increases as the Cr content increases. A similar behavior is observed for c_{HCP} in the studied compositions.

The expressions found for the lattice parameters variation as a function of the amounts of Mn and Cr can be used to analyze structural aspects of these phases and characteristics of the martensitic transformation that takes place between them. Fig. 6 presents the calculated c/a relationship for the HCP phase of Fe-Mn-Cr alloys as a function of Mn for different Cr contents. First, it can be noticed that for each considered amount of Cr, c/a values present a slight variation with the

Table 2
Results of the quadratic fittings of C_i parameters as a function of the Cr content (Eq. (2)).

Lattice constant	Linear fit parameters (as function of Mn)	Quadratic fit parameters (as function of Cr)		
		d_N [10^{-7}(Å/wt%)^3]	e_N [10^{-5}(Å/wt%)^2]	f_N [(Å/wt%)]
a_{FCC}	C_1	−7.84	−1.43	1.202×10^{-3}
	C_2/(wt%)	799.5	24.91	3.5703
a_{HCP}	C_3	87.11	−11.08	7.817×10^{-4}
	C_4/(wt%)	−1077.6	215.971	2.5189
c_{HCP}	C_5	70.63	−6.97	1.120×10^{-3}
	C_6/(wt%)	−811.8	240.158	4.064

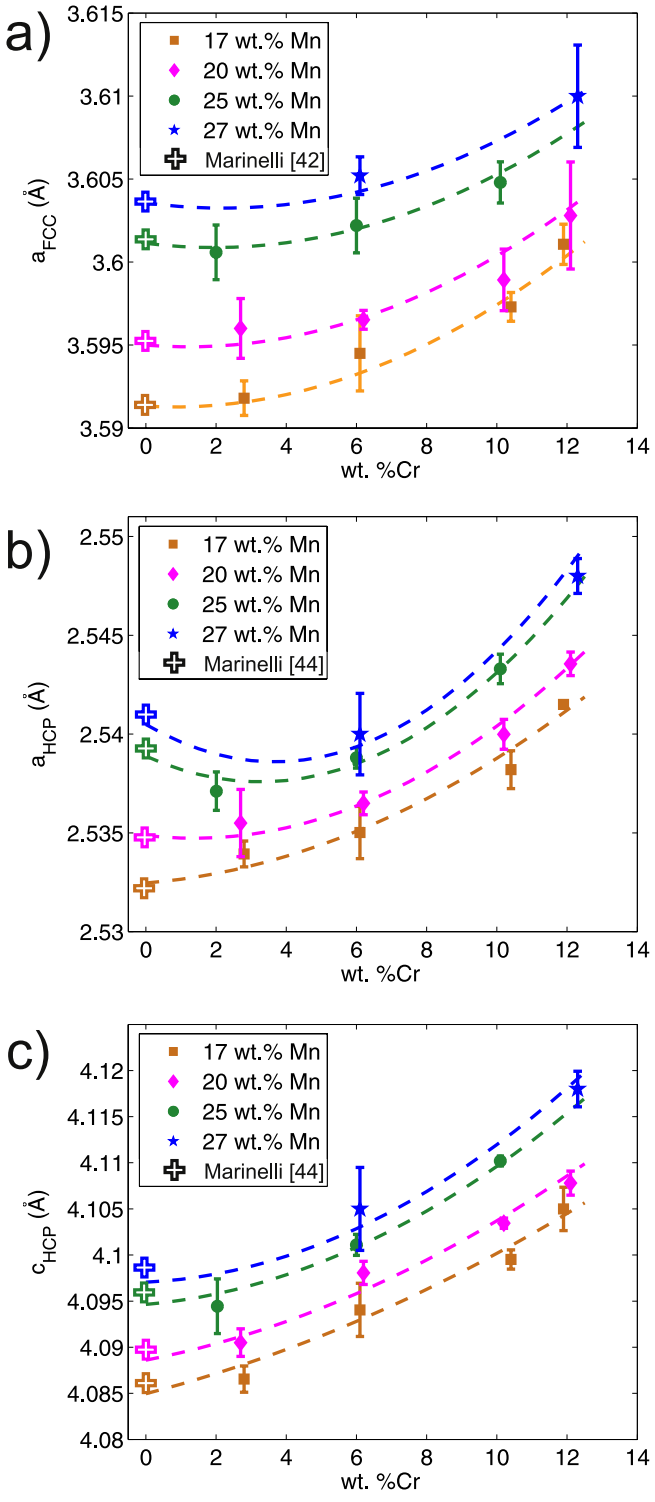

Fig. 5. Calculated variations of the lattice parameters of Fe-Mn-Cr alloys as a function of the Cr content for different amounts of Mn (dashed lines). In each case, experimental values have been included as solid symbols. Cross-shaped symbols correspond to values reported by Marinelli et al. for the Fe-Mn system [52,53]. a) Lattice parameter of the FCC phase. b) and c) Lattice parameters of the HCP phase.

amount of Mn, in line with similar findings in the Fe-Mn system [53]. In all cases c/a values are below than the value 1.633, corresponding to the ideal packing of hard spheres. The addition of Cr tends to increase the c/a relationship towards the ideal value, although it remains significantly lower even for the highest amount of Cr considered.

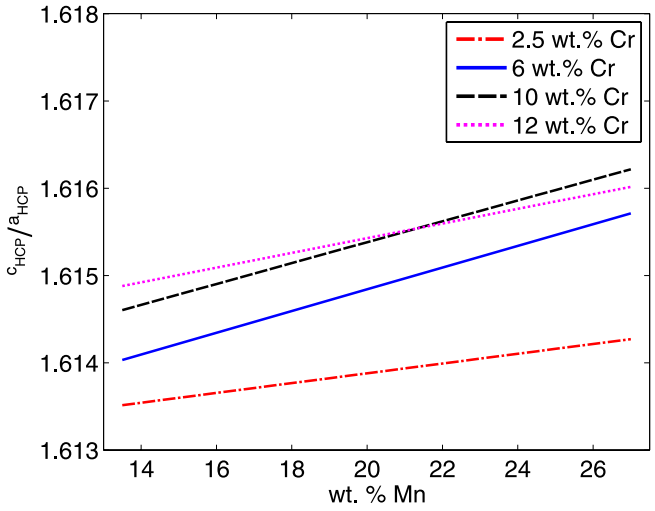

Fig. 6. c/a relationship for the Fe-Mn-Cr alloys HCP phase as a function of Mn for various Cr amounts.

3.3. FCC/HCP relative volume difference

The observed variations in the lattice parameters of FCC and HCP phases can be analyzed from the point of view of the relative volume difference per atom, which could affect the martensitic transformation between these phases. The relative volume difference per atom between these phases is defined as:

$$\frac{dV}{V} = \frac{V_{at}^{FCC} - V_{at}^{HCP}}{V_{at}^{FCC}} \times 100, \tag{3}$$

where V_{at}^{FCC} and V_{at}^{HCP} are the volume per atom of the FCC and HCP phases, respectively. Fig. 7a presents the variation of the relative volume difference as a function of Mn for various Cr contents. Dashed lines correspond to the result of volume changes calculated using Eqs. (1) and (2) while the dots correspond to values obtained from the measured lattice parameters. In all cases, the relative volume change as defined in Eq. 3, is positive, i.e., the material shows a volume contraction during the martensitic γ-ε transition. Alloys with 2.5 wt% Cr and 6 wt% Cr show a tendency to increase the relative volume change as the Mn content increases. This tendency changes with the increment in Cr content (Fig. 7b). In particular, the calculated volume change for alloys containing 12 wt% Cr displays a tendency to decrease with the increment in Mn content. This decrease of the volume change with the increment of Cr in the alloys, as shown in Fig. 7b, opens interesting possibilities from the alloy design perspective.

As it was mentioned before, in all the studied cases the volume per atom is larger in the FCC phase than in the HCP phase. A question remains on whether the FCC/HCP volume change is isotropic or not. As a way to approach this question we can use the expressions found for the variations of lattice parameters in terms of the amount of Mn and Cr (Eqs. (1) and (2)) to calculate the interatomic distances and the close-packed interplanar distance in each structure. Fig. 8a shows the relation between the interatomic distance in HCP (a_{HCP}) and FCC as a function of Mn content for different Cr levels. In the former structure, it directly corresponds to the lattice parameter a_{HCP} while in the FCC phase, the nearest neighbors are located in the [110] direction (d_{110}). Values are below 1, indicating that atoms are closer in the HCP phase. Likewise, the relation between the close-packed interatomic distances can be calculated. In this case, we compared the HCP lattice parameter c_{HCP} which comprises 2 close-packed planes, with the corresponding distance in the [111] direction of FCC (2 d_{111}). The result is presented in Fig. 8b as a function of Mn. Once again, values are below 1 indicating that these planes are closer to each other in HCP than in FCC. The

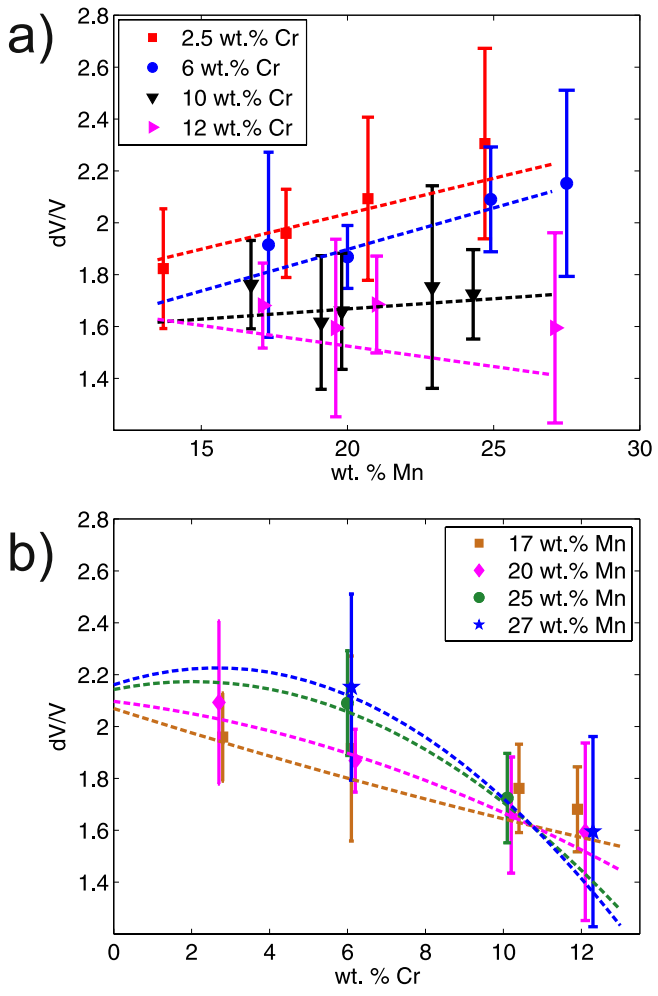

Fig. 7. Relative volume difference (in percent) between the HCP and the FCC parent phase, as defined in Eq. (3). Dotted lines correspond to calculated values and solid dots to present experimental measurements. a) As a function of Mn content for various amounts of Cr. b) As a function of Cr content for various amounts of Mn.

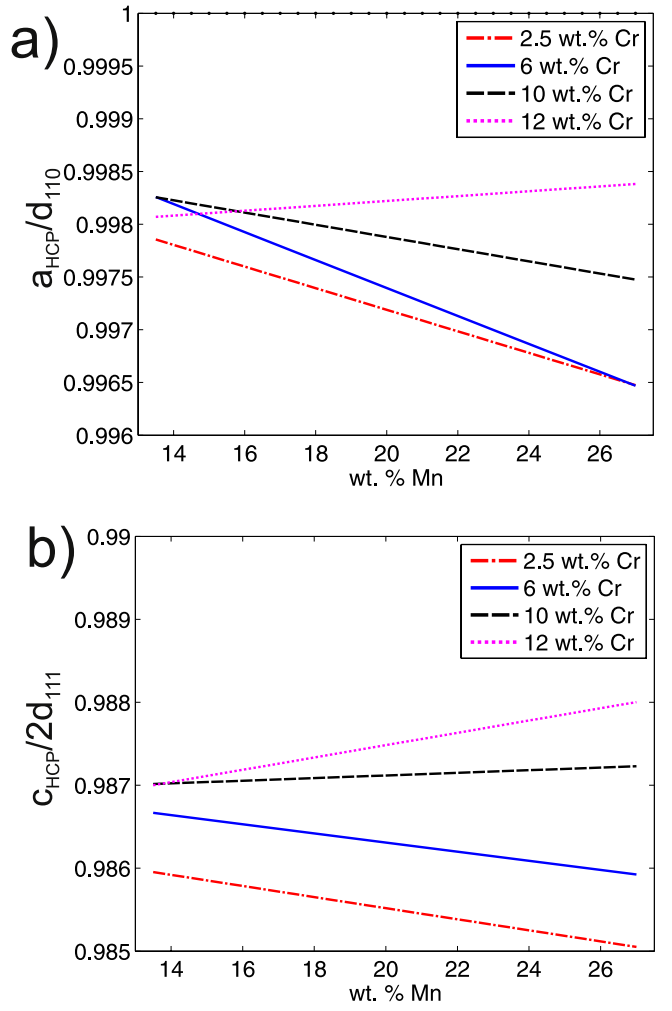

Fig. 8. a) Relation between the interatomic distances of the HCP (a_{HCP}) and FCC (d_{110}) phases as a function of Mn for different Cr contents. b) Relation between the close-packed interatomic distances of the HCP (c_{HCP}) and FCC (2 d_{111}) phases as a function of Mn for different Cr contents.

reduction in the direction perpendicular to the close-packed planes is stronger than that occurring in the densest atomic direction. Then, it is the former contribution the main responsible for the observed volume change. Considering these findings and the results for c/a presented in Fig. 6, we observe that atoms bonds are stronger in HCP. This could indicate that there is a degree of covalent bonding between the metallic species of the alloy. A practical implication of these results is that a harder, more resistant HCP martensite can be expected in this system.

3.4. FCC/HCP strain energy

In 1976 Olson and Cohen presented a model which has been widely used to describe the nucleation of the HCP martensitic structure inside an FCC phase [49]. This model is mainly based on an energy balance which takes place when an embryo of martensite formed by n atomic planes reaches the critical size becoming a nucleus: the driving force of the transformation usually defined as a positive value of the Gibbs energy difference between the FCC and HCP structures ($\Delta G_m^{FCC-HCP}$ defined as $G_m^{HCP} - G_m^{FCC}$) must reach the energetic barriers of the transformation given by the strain energy (E_m^{st}) and the surface energy (E_m^{sur}).

$$\tau(n) = n\rho\left(\Delta G_m^{FCC-HCP} + E_m^{st}\right) + E_m^{sur} \tag{4}$$

Eq. (4) describes the balance of energy, where $\tau(n)$ is the energy change corresponding to an HCP nucleus, which depends on the number of planes (n), being ρ the atomic density in a compact plane in moles per unit area. This atomic density can be obtained by using the following equation:

$$\rho = \frac{4}{\sqrt{3}\cdot N_A \cdot (a_{FCC})^2}\ (\mathrm{mol/m^2}) \tag{5}$$

Eq. (4) could be used to obtain the stacking fault energy (SFE) by considering only the first two planes which form the fault, i.e., SFE $= \tau$ when $n = 2$. On the other hand, it is also possible to calculate the critical size of the HCP nucleus, which would correspond to the n value where $\tau(n) = 0$.

The mentioned analysis has been used to describe nucleation in the FCC-HCP transformation in different alloys by several researchers. For example, this approach has been used in a recent paper on Fe-Mn [55], works on ternary Fe-Mn-Si [50,56] and a new study on Fe-Mn alloys [57]. Concerning Eq. (4), different methods have been suggested to obtain the driving force of the transformation. A usual approach consists in modeling the Gibbs energy of each phase using thermodynamic analysis, although this methods lead to a relatively large range of values in similar alloys [50,57]. The surface energy can be modeled in a relatively easy way and values close to 20 mJ/m^2 have been obtained [50]. The strain energy term requires the analysis of the micromechanics associated to the nucleation and the use of the linear elasticity theory to

estimate it. In what follows it will be shown how the knowledge of precise values of the lattice parameters of each phase and the volume change between them can be used to estimate the elastic strain energy term. A similar analysis has been used in Ref. [50] to determine the strain energy term in Fe-Mn alloys. In that case, the strain energy accounts for the 20% of the involved driving force at the martensitic transformation temperature. Therefore, evaluating the strain energy is relevant in order to analyze the nucleation of the HCP martensite.

Following the same procedure used in [50], it is possible to estimate the strain energy based on the linear elastic theory and considering the nucleation of a coherent plate in an isotropic medium. This estimation sums up two contributions, an energy term associated to a dilatational component E_m^{dil} and a shear component E_m^{sh} [50]:

$$E_m^{st} = E_m^{dil} + E_m^{sh} \tag{6}$$

In particular, the dilatational component mainly depends on the volume change between FCC and HCP (ΔV_m) relative to the matrix volume (V_m^{FCC}), and also on the elastic constants, i.e., the shear modulus (μ) and the Poisson coefficient ν as shown in Eq. (7) [50]:

$$E_m^{dil} = \frac{2(1-\nu)}{9(1+\nu)} \cdot \mu \cdot V_m^{FCC} \left(\frac{\Delta V_m}{V_m^{FCC}} \right)^2 \tag{7}$$

The shear component can be obtained using the following expression [50]:

$$E_m^{sh} = \frac{2(7-5\nu)}{45(1-\nu)} \cdot \mu \cdot V_m^{FCC} \cdot (\varepsilon_{33})^2, \tag{8}$$

where ε_{33} is the diagonal component of the strain matrix along the c axis. Eq. (8) takes into consideration that the main contribution to variation in lattice parameters takes place along the c axis of the HCP phase in the same way as it occurs in the binary Fe-Mn system. In order to perform a numeric estimation of both contributions to the strain energy, the lattice parameters presented in Table 1 have been used. In addition, as a first approximation, the elastic constants reported for binary alloys were used ($\nu = 1/3$ and $\mu = 5.2 \times 10^{10}$ N/m^2) [50].

Fig. 9 shows the results obtained using Eqs. (7) and (8). No noticeable effect of Mn content is observed. The effect of Cr on the strain energy and both contributions, dilatational and shear ones, are shown in Fig. 9a and b. It is clearly observed that these energy terms decrease as Cr content increases. The obtained values of the energy terms for null Cr content were calculated using the lattice parameters measured by Marinelli et al. in binary Fe-Mn alloys [52]. It is remarkable that these values agree with those obtained using the data obtained here for the ternary Fe-Mn-Cr system extrapolated to null Cr content by using the tendencies presented in Fig. 9.

From the results shown in Fig. 9 and considering the effect of Cr on the volume change between FCC and HCP, it can be expected that the addition of this element favorably affects the shape memory effect since it should favor reversibility of the transformation.

Finally, an interesting and significant output of the present manuscript is that for the analyzed range of compositions the strain energy reaches values close to 40 J/mol, an amount which must be taken into consideration if the involved driving forces are close to 200 J/mol as it has been reported for Fe-Mn binary alloys [50].

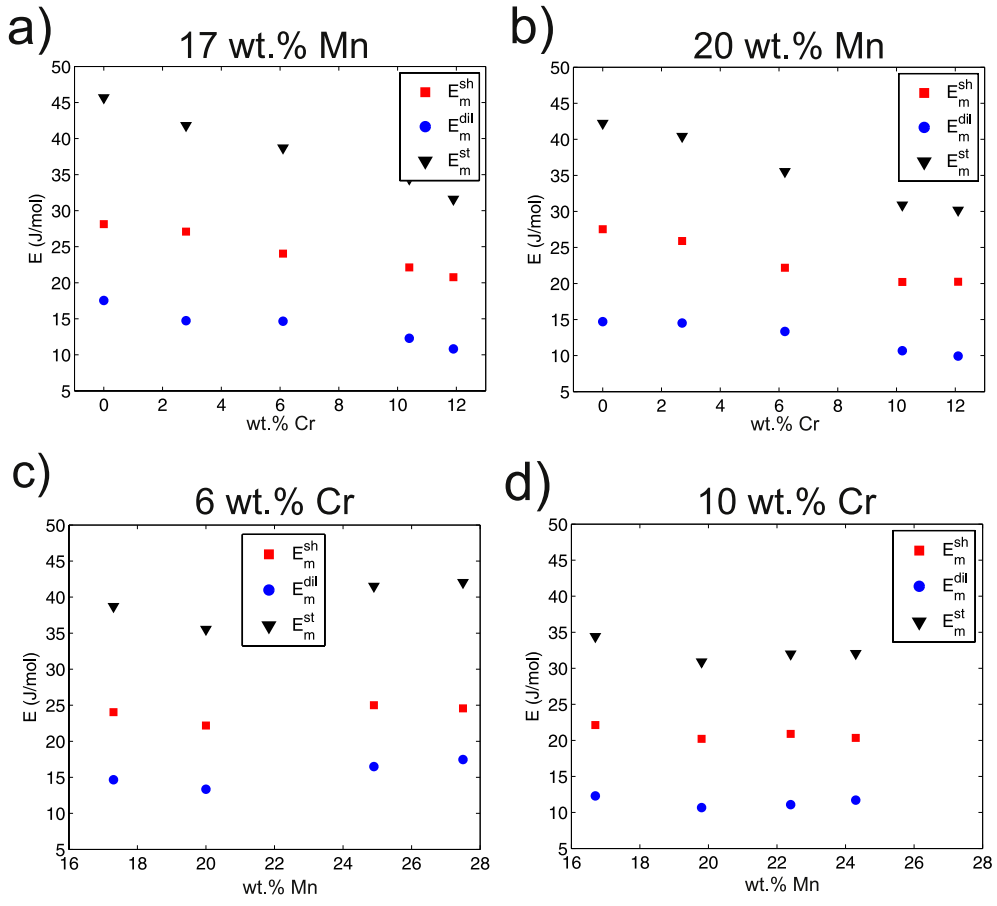

Fig. 9. Calculated strain energy of Fe-Mn-Cr alloys as a function of the Cr content, a) at 17 wt% Mn, b) at 20 wt% Mn, and as a function of the Mn content. c) at 6 wt% Cr and d) at 10 wt% Cr.

4. Conclusions

Lattice parameters have been measured for the BCC, FCC and HCP phases of quenched Fe-Mn-Cr alloys in an extended range where the FCC/HCP martensitic transformation takes place in this system. The following are the most remarkable points:

- BCC lattice parameters do not show a strong dependence with the alloy composition while FCC and HCP lattice parameters do: these variations where analyzed in terms of the Mn and Cr contents of the alloys and expressions where found that closely describe the experimental results. All measured parameters (a_{FCC}, a_{HCP} and c_{HCP}) tend to increase with the increment of Mn amount at constant Cr content.
- The HCP phase is denser than the FCC structure and the volume change is strongly associated to a change in the interplanar distance between close-packed planes.
- Expressions have been proposed that allowed calculating the volume per atom for each structure and thus, evaluating the volume change associated to the FCC/HCP martensitic transformation in the whole range of studied compositions: the obtained tendencies show that it is possible to reduce the volume change between FCC and HCP by the addition of Cr.
- The addition of Cr decreases the strain energy which is one of the main energy barriers to the transformation. It can then be expected a positive effect of Cr on the shape memory properties of Fe-Mn-based alloys.

Acknowledgements

Dr. M.A. Arribere performed all neutron activation chemical analyses of alloys. Quartz capsules were prepared by Mr. E. Aburto and Mr. M.J. Isla. Dr. F. Castro kindly helped with X-Ray diffractometer operation. Research funding was provided by ANPCyT, Argentina (PICT 2012-0884), CONICET, Argentina (PIP 2015-0521) and UNCUYO (06/C516).

References

[1] Y.H. Wen, H.B. Peng, D. Raabe, I. Gutierrez-Urrutia, J. Chen, Y.Y. Du, Large recovery strain in Fe-Mn-Si-based shape memory steels obtained by engineering annealing twin boundaries, Nat. Commun. 5 (2014) 4964, https://doi.org/10.1038/ncomms5964.
[2] A. Sato, H. Kubo, T. Maruyama, Mechanical properties of Fe–Mn–Si based SMA and the application, Mater. Trans. 47 (2006) 571–579, https://doi.org/10.2320/matertrans.47.571.
[3] A.V. Druker, A. Perotti, I. Esquivel, J. Malarría, A manufacturing process for shaft and pipe couplings of Fe–Mn–Si–Ni–Cr shape memory alloys, Mater. Des. 1980–2015 (56) (2014) 878–888, https://doi.org/10.1016/j.matdes.2013.11.032.
[4] H. Otsuka, H. Yamada, T. Maruyama, H. Tanahashi, S. Matsuda, M. Murakami, Effects of alloying additions on Fe-Mn-Si shape memory alloys, ISIJ Int. 30 (1990) 674–679, https://doi.org/10.2355/isijinternational.30.674.
[5] X.M. Zhu, Y.S. Zhang, Investigation of the electrochemical corrosion behavior and passive film for Fe-Mn, Fe-Mn-al, and Fe-Mn-Al-Cr alloys in aqueous solutions, Corrosion 54 (1998) 3–12, https://doi.org/10.5006/1.3284826.
[6] Y.N. Petrov, On the electron structure of Mn–, Ni– and Cr–Ni–Mn austenite with different stacking fault energy, Scr. Mater. 53 (2005) 1201–1206, https://doi.org/10.1016/j.scriptamat.2005.07.002.
[7] Y. Watanabe, H. Sato, Y. Nishino, I.S. Kim, Training effects on damping capacity in Fe-Mn and Fe-Mn-Cr alloys, Mater. Sci. Forum 638–642 (2010) 2201–2206, https://doi.org/10.4028/www.scientific.net/MSF.638-642.2201.
[8] M. Sade, A. Baruj, H.E. Troiani, Fcc/hcp martensitic transformation temperatures and thermal cycling evolution in Fe-Mn-Cr alloys, New Dev. Metall. Appl. High Strength Steels Proc. Int. Conf. New Dev. Metall. Appl. High Strength Steels 2 (2008) 1183–1191.
[9] P. Franke, H.J. Seifert (Eds.), Ternary Steel Systems: Phase Diagrams and Phase Transition Data, Springer Berlin Heidelberg, Berlin, Heidelberg, 2012https://doi.org/10.1007/978-3-540-88142-1.
[10] Y. Murata, K. Koyama, Y. Matsumoto, M. Morinaga, N. Yukawa, Equilibrium phase diagram of Fe-Cr-Mn ternary system, ISIJ Int. 30 (1990) 927–936, https://doi.org/10.2355/isijinternational.30.927.
[11] N.A. Sorokina, A.P. Shlyamnev, Corrosion-resistant Cr—Mn steels with elevated strength: an alternative to Cr—Ni steels, Met. Sci. Heat Treat. 41 (1999) 260–265, https://doi.org/10.1007/BF02468240.
[12] E.S. Gorkunov, S.V. Gladkovskii, S.M. Zadvorkin, S.Y. Mitropol'skaya, D.I. Vichuzhanin, Evolution of magnetic properties of Fe-Mn and Fe-Mn-Cr steels with different stability of austenite during plastic deformation, Phys. Met. Metallogr. 105 (2008) 343–350, https://doi.org/10.1134/S0031918X08040054.
[13] L. Bracke, G. Mertens, J. Penning, B.C. De Cooman, M. Liebeherr, N. Akdut, Influence of phase transformations on the mechanical properties of high-strength austenitic Fe-Mn-Cr steel, Metall. Mater. Trans. A 37 (2006) 307–317, https://doi.org/10.1007/s11661-006-0002-5.
[14] L. Remy, A. Pineau, Twinning and strain-induced F.C.C. → H.C.P. transformation in the Fe-Mn-Cr-C system, Mater. Sci. Eng. 28 (1977) 99–107, https://doi.org/10.1016/0025-5416(77)90093-3.
[15] L.M. Guerrero, P. La Roca, F. Malamud, A. Baruj, M. Sade, Composition effects on the fcc-hcp martensitic transformation and on the magnetic ordering of the fcc structure in Fe-Mn-Cr alloys, Mater. Des. 116 (2017) 127–135, https://doi.org/10.1016/j.matdes.2016.12.003.
[16] M. Schwind, J. Källqvist, J.-O. Nilsson, J. Agren, H.-O. Andrén, σ-Phase precipitation in stabilized austenitic stainless steels, Acta Mater. 48 (2000) 2473–2481, https://doi.org/10.1016/S1359-6454(00)00069-0.
[17] H.E. Troiani, M. Sade, G. Bertolino, A. Baruj, Martensitic transformation temperatures and microstructural features of FeMnCr alloys, Eur. Symp. Martensitic Transform, EDP Sciences 2009, p. 06002, https://doi.org/10.1051/esomat/200906002.
[18] V. Mertinger, M. Benke, E. Nagy, Effect of Cr content on the TWIP behavior in Fe-Mn-Cr steels, Mater. Today Proc. 2 ((2015) S673–S676, https://doi.org/10.1016/j.matpr.2015.07.373.
[19] V. Mertinger, M. Benke, E. Nagy, T. Pataki, Reversible characteristics and cycling effects of the ε ↔ γ martensitic transformations in Fe-Mn-Cr Twip/Trip steels, J. Mater. Eng. Perform. 23 (2014) 2347–2350, https://doi.org/10.1007/s11665-014-1025-5.
[20] V.V. Berezovskaya, Y.A. Raskovalova, E.A. Merkushkin, R.Z. Valiev, Twip-effect in nickel-free high-nitrogen austenitic Cr – Mn steels, Met. Sci. Heat Treat. 57 (2016) 656–662, https://doi.org/10.1007/s11041-016-9938-2.
[21] P.R. Rao, V.V. Kutumbarao, Developments in austenitic steels containing manganese, Int. Mater. Rev. 34 (1989) 69–92.
[22] A. Nyilas, K. Weiss, G. Grikurov, N. Zoidze, Tensile, fracture, and fatigue crack growth rate behavior of high manganese steels, AIP Conf. Proc. 824 (2006) 130–137, https://doi.org/10.1063/1.2192343.
[23] P. Sahu, S.K. Shee, A.S. Hamada, L. Rovatti, T. Sahu, B. Mahato, S. Ghosh Chowdhury, D.A. Porter, L.P. Karjalainen, Low strain rate deformation behavior of a Cr–Mn austenitic steel at −80 °C, Acta Mater. 60 (2012) 6907–6919, https://doi.org/10.1016/j.actamat.2012.07.055.
[24] U.R. Lenel, B.R. Knott, Structure and properties of corrosion and wear resistant Cr-Mn-N steels, Metall. Mater. Trans. A 18 (1987) 847–855, https://doi.org/10.1007/BF02646926.
[25] P. Behjati, A. Kermanpur, A. Najafizadeh, H.S. Baghbadorani, Effect of annealing temperature on nano/ultrafine grain of Ni-free austenitic stainless steel, Mater. Sci. Eng. A 592 (2014) 77–82, https://doi.org/10.1016/j.msea.2013.10.087.
[26] Z. Lv, P. Cai, T. Yu, Y. Jin, H. Zhang, W. Fu, T. Zhai, Fatigue behaviors and damage mechanism of a Cr-Mn-N austenitic steel, J. Alloys Compd. 691 (2017) 103–109, https://doi.org/10.1016/j.jallcom.2016.08.228.
[27] P. Fenici, D. Boerman, V. Coen, E. Lang, C. Ponti, W. Schüle, Properties of Cr-Mn austenitic stainless steels for fusion reactor applications, Nucl. Eng. Des. Fusion 1 (1984) 167–183, https://doi.org/10.1016/0167-899X(84)90038-7.
[28] G. Piatti, S. Matteazzi, G. Petrone, Time independent tensile behaviour of a high manganese steel selected as a candidate material in conceptual tokamak fusion reactor designs, Nucl. Eng. Des. Fusion 2 (1985) 391–406, https://doi.org/10.1016/0167-899X(85)90027-8.
[29] K. Miyahara, D.-S. Bae, T. Kimura, Y. Shimoide, Y. Hosoi, Strength properties and microstructure of high Mn-Cr austenitic steels as potential high temperature materials, ISIJ Int. 36 (1996) 878–882, https://doi.org/10.2355/isijinternational.36.878.
[30] M. Onozuka, T. Saida, S. Hirai, M. Kusuhashi, I. Sato, T. Hatakeyama, Low-activation Mn–Cr austenitic stainless steel with further reduced content of long-lived radioactive elements, J. Nucl. Mater. 255 (1998) 128–138, https://doi.org/10.1016/S0022-3115(98)00031-2.
[31] Y. Suzuki, T. Saida, F. Kudough, Low activation austenitic Mn-steel for in-vessel fusion materials, J. Nucl. Mater. 258 (1998) 1687–1693.
[32] J.C. Rawers, Alloying effects on the microstructure and phase stability of Fe–Cr–Mn steels, J. Mater. Sci. 43 (2008) 3618–3624, https://doi.org/10.1007/s10853-008-2576-3.
[33] A. Kermanpur, P. Behjati, J. Han, A. Najafizadeh, Y.-K. Lee, A microstructural investigation on deformation mechanisms of Fe–18Cr–12Mn–0.05 C metastable austenitic steels containing different amounts of nitrogen, Mater. Des. 82 (2015) 273–280, https://doi.org/10.1016/j.matdes.2015.05.075.
[34] S. Cotes, M. Sade, A.F. Guillermet, Fcc/Hcp martensitic transformation in the Fe-Mn system: experimental study and thermodynamic analysis of phase stability, Metall. Mater. Trans. A 26 (1995) 1957–1969, https://doi.org/10.1007/BF02670667.
[35] N. Zotov, M. Pfund, E. Polatidis, A.F. Mark, E.J. Mittemeijer, Change of transformation mechanism during pseudoelastic cycling of NiTi shape memory alloys, Mater. Sci. Eng. A 682 (2017) 178–191, https://doi.org/10.1016/j.msea.2016.11.052.
[36] L. Isola, P. La Roca, C. Sobrero, V. Fuster, P. Vermaut, J. Malarría, Study of the load-biased martensitic transformation strain and stability of Ni50 — x-Ti-Cox strips obtained by twin-roll and standard casting techniques, Mater. Des. 107 (2016) 511–519, https://doi.org/10.1016/j.matdes.2016.06.049.
[37] H. Fu, S. Xu, H. Zhao, H. Dong, J. Xie, Cyclic stress-strain response of directionally solidified polycrystalline Cu-Al-Ni shape memory alloys, J. Alloys Compd. 714 (2017) 154–159.

[38] M. Sade, P. La Roca, F. De Castro Bubani, F.C. Lovey, V. Torra, A. Yawny, Pseudoelastic cycling between austenite, 18R and 6R phases in CuAlBe single crystals, Mater. Today Proc. 2 (Suppl. 3) (2015) S719–S722.
[39] K. Ando, T. Omori, I. Ohnuma, R. Kainuma, K. Ishida, Ferromagnetic to weak-magnetic transition accompanied by bcc to fcc transformation in Fe–Mn–Al alloy, Appl. Phys. Lett. 95 (2009), 212504. https://doi.org/10.1063/1.3266848.
[40] T. Omori, K. Ando, M. Okano, X. Xu, Y. Tanaka, I. Ohnuma, R. Kainuma, K. Ishida, Superelastic effect in polycrystalline ferrous alloys, Science 333 (2011) 68–71, https://doi.org/10.1126/science.1202232.
[41] M. Vollmer, C. Segel, P. Krooß, J. Günther, L.W. Tseng, I. Karaman, A. Weidner, H. Biermann, T. Niendorf, On the effect of gamma phase formation on the pseudoelastic performance of polycrystalline Fe-Mn-Al-Ni shape memory alloys, Scr. Mater. 108 (2015) 23–26, https://doi.org/10.1016/j.scriptamat.2015.06.013.
[42] P. La Roca, J. Medina, C.E. Sobrero, M. Avalos, J.A. Malarria, A. Baruj, M. Sade, Effects of B2 nanoprecipitates on the phase stability and pseudoelastic behavior of Fe-Mn-Al-Ni shape memory alloys, MATEC Web of Conferences, 33, 2015, p. 04005.
[43] T. Niendorf, F. Brenne, P. Krooß, M. Voller, J. Günter, D. Schwarze, H. Biermann, Microstructural evolution and functional properties of Fe-Mn-Al-Ni shape memory alloy processed by selective laser melting, Metall. Mater. Trans. A 47 (6) (2016) 2569–2573, https://doi.org/10.1007/s11661-016-3412-z.
[44] T. Omori, H. Iwazako, R. Kainuma, The abnormal grain growth induced by cyclic heat treatment in Fe-Mn-Al-Ni superelastic alloy, Mater. Des. 101 (2016) 263–269, https://doi.org/10.1016/j.matdes.2016.04.011.
[45] M. Vollmer, P. Krooß, M.J. Kriegel, V. Klemm, C. Somsen, H. Ozcan, I. Karaman, A. Weidner, D. Rafaja, H. Biermann, T. Niendorf, Cyclic degradation in bamboo-like Fe-Mn-Al-Ni shape memory alloys-the role of grain orientation, Scr. Mater. 114 (2016) 156–160, https://doi.org/10.1016/j.scriptamat.2015.12.007.
[46] P. La Roca, A. Baruj, C.E. Sobrero, J.A. Malarria, M. Sade, Nanoprecipitation effects on phase stability of Fe-Mn-Al-Ni alloys, J. Alloys Compd. 708 (2017) 422–427.
[47] S. Reeh, M. Kasprzak, C.D. Klusmann, F. Stalf, D. Music, M. Ekholm, I.A. Abrikosov, J.M. Schneider, Elastic properties of fcc Fe–Mn–X (X = Cr, Co, Ni, Cu) alloys studied by the combinatorial thin film approach and *ab initio* calculations, J. Phys. Condens. Matter 25 (2013), 245401. https://doi.org/10.1088/0953-8984/25/24/245401.
[48] K. Tamarat, V. Stambouli, T. Bouraoui, B. Dubois, Structural study of Fe-Mn-Si and Fe-Mn-Cr shape memory steels, J. Phys. IV 01 (1991) (C4-347–C4-353) https://doi.org/10.1051/jp4:1991452.
[49] G.B. Olson, M. Cohen, A general mechanism of martensitic nucleation: part I. General concepts and the FCC → HCP transformation, Metall. Trans. A. 7 (1976) 1897–1904, https://doi.org/10.1007/BF02659822.
[50] S.M. Cotes, A.F. Guillermet, M. Sade, Fcc/Hcp martensitic transformation in the Fe-Mn system: part II. Driving force and thermodynamics of the nucleation process, Metall. Mater. Trans. A 35 (2004) 83–91, https://doi.org/10.1007/s11661-004-0111-y.
[51] R.A. Young (Ed.), The Rietveld Method, International Union of Crystallography, Chester, England; Oxford; New York, 1995https://doi.org/10.1080/00140139508925159.
[52] P. Marinelli, M. Sade, A. Baruj, A.F. Guillermet, Lattice parameters of metastable structures in quenched Fe-Mn alloys. Pt. I. Experimental techniques, bcc and fcc phases, Z. Metallkd. 91 (2000) 957–962.
[53] P. Marinelli, A. Baruj, A.F. Guillermet, M. Sade, Lattice parameters of metastable structures in quenched Fe-Mn alloys. Part II: hcp phase, Z. Met. 92 (2001) 489–493.
[54] P. Marinelli, M. Sade, A. Fernández Guillermet, On the structural changes accompanying the fcc/hcp martensitic transformation in Fe–Mn–Co alloys, Scr. Mater. 46 (2002) 805–810, https://doi.org/10.1016/S1359-6462(02)00080-5.
[55] D.T. Pierce, J.A. Jiménez, J. Bentley, D. Raabe, C. Oskay, J.E. Wittig, The influence of manganese content on the stacking fault and austenite/ε-martensite interfacial energies in Fe–Mn–(Al–Si) steels investigated by experiment and theory, Acta Mater. 68 (2014) 238–253, https://doi.org/10.1016/j.actamat.2014.01.001.
[56] J. Xuejun, Z. Jihua, T.Y. Hsu, Thermodynamic calculation of stacking fault energy in Fe–Mn–Si shape memory alloys, Mater. Des. 21 (2000) 537–539, https://doi.org/10.1016/S0261-3069(00)00006-6.
[57] S.T. Pisarik, D.C.V. Aken, Thermodynamic driving force of the γ → ε transformation and resulting MS temperature in high-Mn steels, Metall. Mater. Trans. A 47 (2016) 1009–1018, https://doi.org/10.1007/s11661-015-3265-x.